NASA TECHNICAL MEMORANDUM

NASA TM X-71613

NASA TM X-71613

SPINNING MODE SOUND PROPAGATION IN DUCTS WITH ACOUSTIC TREATMENT

by Edward J. Rice
Lewis Research Center
Cleveland, Ohio 44135

TECHNICAL PAPER to be presented at
Eighty-eighth Meeting of the Acoustical Society of America
St. Louis, Missouri, November 5-8, 1974

SPINNING MODE SOUND PROPAGATION IN DUCTS WITH ACOUSTIC TREATMENT

by Edward J. Rice

Lewis Research Center

SUMMARY

Recent acoustic data have shown larger noise attenuations than predicted for acoustically treated aircraft engine inlets without splitter rings. These encouraging data have stimulated a more detailed theoretical study of the acoustic propagation of spinning modes in acoustically treated open circular ducts. In addition, the suppressor with splitter rings was modeled by using the rectangular approximation to the annular duct. The theoretical models were used to determine optimum impedance and maximum attenuation for several spinning lobe numbers from 0 to 50. Some interesting results of the analysis are that for circular ducts the maximum possible attenuation and the optimum wall impedance are strong functions of the lobe number. For annular ducts the attenuation and optimum wall impedance are insensitive to the spinning lobe number for well cut-on modes. The above results help explain why suppressors with splitter rings have been quite effective in spite of the lack of detailed information on the noise source modal structure. Conversely, effective use of outer wall treatment alone will require expanded knowledge of the noise source structure. Approximate solutions are presented to help interpret the more exact theoretical results.

INTRODUCTION

Noise suppressor design procedures have evolved over the past several years providing quite predictable suppressor configurations for aircraft engine inlet and exhaust ducts with splitter rings. These procedures have evolved from empirical correlation of extensive noise

attenuation tests in flow ducts and from theoretical studies of sound propagation in ducts with acoustic treatment. The sound propagation theory has used quite simple noise input functions such as a plane wave (refs. 1 to 3) or the axisymmetric least-attenuated mode (ref. 4). These simple models have provided very good design procedures as long as splitter rings were used. Not much attention was paid to the suspected, but largely undefined, complex modal structure of the fan noise source, and it really did not seem to make much difference that this complexity was ignored. It has been known for several years that spinning duct modes would be produced by rotor-stator interaction (ref. 5) and by inlet distortion-rotor interaction (refs. 6 and 7). Yet flow duct tests which did not contain this type of mode produced empirical design procedures that resulted in predictable splitter ring suppressors.

Recent noise data from aircraft engine inlets showing surprisingly high suppression with only outer wall acoustic treatment as well as the strong incentive to reduce noise suppressor pressure losses have stimulated renewed interest in the role of modal structure in noise suppressor theory. Neither axisymmetric sound propagation theory nor flow duct empericism has explained the large noise attenuations which were observed. It was hypothesized that the spinning mode character of sound does indeed make a difference in the performance of inlet suppressors with treatment on the outer wall alone.

The propagation of spinning modes in soft-walled ducts has been studied in the past (refs. 8 to 10 are examples), but a general design procedure has not resulted from these studies. It appears that a thorough theoretical and experimental study of spinning mode sound propagation in acoustically treated circular ducts is needed. This paper represents an attempt to initiate this theoretical study to provide rules for optimization of duct treatment and to explain some of the observed differences between splitter ring designs and outer-wall treatment alone configurations.

SYMBOLS

A	constant multiplier (see eq. (9))
a	one-half of lined duct height, m
B_θ	optimum resistance coefficient for circular ducts (see eq. (36))
B_χ	optimum reactance coefficient for circular ducts (see eq. (37))
c	speed of sound, m/sec
D	circular duct diameter, m
D_m	attenuation coefficient (see eq. (60))
E	acoustic power, W
f	frequency, Hz
H	height between lined walls, m
J_m	Bessel function of first kind of order m
k	integer variable
L	acoustically treated duct length, m
M	uniform steady flow Mach number
M_t	lobe pattern tip Mach number
m	lobe pattern number
P	part of acoustic pressure which is function of transverse coordinates (r, Φ or y, z) (see eq. (2)), N/m^2
$\mathscr{P}$	part of acoustic pressure which is function of coordinate between acoustically treated surfaces (r or y), N/m^2
p	acoustic pressure, N/m^2
Q	$1 + iM(\sigma + i\tau)$
R	amplitude of eigenvalue α
r	radial coordinate, m
r_i	inner radius of an annulus, m
r_o	outer radius of an annulus, m

t	time, sec
V_{gx}	axial group velocity, m/sec
V_{px}	axial phase velocity, m/sec
v	acoustic particle velocity (vector), m/sec
x	axial coordinate, m
Y_m	Bessel function of second kind, of order m
y	transverse coordinate (see fig. 3), m
Z	liner acoustic impedance (see eq. (11)), $kg/m^2/sec$
z	transverse coordinate (see fig. 3), m
α	complex eigenvalue ($\alpha = Re^{i\varphi}$)
β	transverse dimension (either D or H)
δ	radius ratio, r_i/r_o
ζ	dimensionless acoustic impedance, $Z/\rho c$
η	frequency parameter, fH/c or fD/c
θ	specific acoustic resistance, real (ζ)
ρ	density, kg/m^3
σ	attenuation coefficient
τ	propagation coefficient
Φ	angular coordinate, rad
φ	phase of eigenvalue
χ	specific acoustic reactance, imag (ζ)
ω	circular frequency, rad/sec

Subscripts:

j	j^{th} radial mode
r	radial component
w	value at the wall

INLET SUPPRESSOR DATA COMPARED WITH THEORY

The motivation for this study came from observation of experimental data from inlet suppressors without splitter rings. Samples of these data are shown in figures 1 and 2.

Sound power attenuation spectra from suppressors tested with NASA Lewis Fan C are shown in figure 1. Fan C is a high tip speed (472 m/sec, 1550 fps), 1.74-meter (68.3-in.) diameter, single fan stage with 26 rotor blades and 60 stator blades (ref. 11). Two attenuation spectra are shown: wall treatment plus three splitter rings; and wall treatment only. Two interesting points about the data should be noted. First, the wall treatment alone configuration is very effective. At high frequencies, near the blade passage frequency ($\approx$2000 Hz), the large attenuation ($\approx$8 dB) obtained cannot be explained by axisymmetric sound propagation theory. Second, at low frequencies where multiple pure tones dominate ($\approx$800 Hz peak), not only is the large attenuation unexplainable by axisymmetric theory, but the splitter rings make very little difference in the attenuation. The insignificant effect of the rings for this type of sound is probably due to the radial pressure distribution of the sound. These questions will be considered again after the spinning mode propagation theory is developed herein.

A number of normalized peak attenuation data points are shown in figure 2 along with three theoretical curves. The maximum sound power attenuation is seen to be normalized by the quantity L/β. The length L is the length of acoustic treatment while β is a radial dimension. The dimension β is the duct diameter for open circular ducts and the duct height between treated surfaces for annular or rectangular ducts. Note that β occurs also in the abscissa (frequency parameter) and should be similarly interpreted there. Maximum sound power attenuation will be explained in more detail later (or see also ref. 1). For now, it can be simply considered as the normalized peak experimental or theoretical sound power attenuation. The theoretical maximum attenuation is obtained with the walls having a particular acoustic impedance (optimum impedance) at a particular sound frequency. This optimum impedance may differ for various duct geometries or for different modal distributions which will be discussed in more detail later.

Two of the theoretical curves represent the largest possible attenuation for circular and rectangular ducts when only the least-attenuated mode is present in these ducts. The third curve shows the maximum attenuation if a plane wave were impressed upon the liner at one end. The least-attenuated mode, often thought of as the most conservative indication of liner performance, is seen to potentially damp faster than the plane wave input. A combination of modes must be excited to match this plane wave input in a soft-walled duct (since a plane wave is not a soft wall solution), and this conglomerate is less readily attenuated than the so-called least-attenuated mode.

It should be noted that the curves of figure 2 do not represent an attenuation spectrum which could be obtained in practice. Each point on the curve represents a liner with optimized wall impedance. No real liner could track this optimum impedance over a frequency range. At most, a real liner could reach these theoretical limits at one frequency only. The theoretical curves were generated without grazing flow ($M = 0$) but they will not change with flow in the region where the attenuation is falling off with η (ref. 3). This lack of dependence on M will be shown in a later section. The $L/H = 4$ plane wave solution was shown since it is typical of the splitter ring suppressors tested. Small changes would occur for other values of L/H (ref. 3).

Some interesting observations can be made by comparing the data with their respective theoretical limits. First, the rectangular flow duct data agree quite well with the rectangular duct theory. The theoretical curve in this frequency range is not influenced very much by the type of modal distribution (plane wave, equal energy, equal amplitude, etc.) existing in the duct. This is due to the small number of propagating modes which could exist over this frequency range (i.e., from two to five modes).

The second set of data (engine or fan inlet with splitters) might also be compared to the rectangular duct theory. A rectangular duct should be a fairly good approximation to at least the outer annulus (which should carry most of the acoustic power) of a splitter ring suppressor which typically has a radius ratio of about 0.8. These attenuation values are

seen to be quite low (about one-fourth) with respect to the theory.

There were several reasons why this difference between theory and experiment may have occurred. The first was intentional; the two sides of the annular passage were designed for different frequencies so as to broaden the bandwidth of sound attenuation. Thus, at any given frequency the entire treated area could not be working at optimum as was the liner for the theoretical curves. Several uncontrollable phenomena were probably also degrading the liner performance. The liner impedance models are not exact, and it would indeed be difficult to construct a liner which was truly optimum. Also, the boundary layer refraction effect was not considered in the liner design. Whatever the reason, it is not too surprising to find experimental attenuation levels well below a theoretically predicted maximum. It is logical to consider the theory as an ideal upper limit and to use theoretical trends for extrapolation from the observed experimental data. This procedure has subsequently produced quite predictable liner designs where splitter rings are used.

The third set of data (wall treatment only) is seen to be an order of magnitude above the axisymmetric propagation theoretical estimate for circular ducts. It is probable that data could be obtained which would be even higher if the walls had been truly optimized. These data are quite easily explained if one accepts that the sound is mainly concentrated in spinning modes, since these modes damp faster than the axisymmetric mode theory of figure 2 would suggest. However, spinning modes should also exist with splitter rings; and at first one might expect that these modes should also damp faster than the axisymmetric modes. The data of course deny this conclusion. It will be shown after the development of the spinning mode theory that the spinning mode properties are largely irrelevant in the splitter ring case, but are the crucial factor in the case of wall-treatment only.

SPINNING MODE PROPAGATION THEORY

Certain assumptions are common in all of the theoretical development which follows. The steady flow is uniform everywhere in the duct.

Boundary layers are sufficiently small so that their effect may be neglected. The soft walls are assumed point reacting and of uniform impedance. These assumptions imply that no waves are propagating within the liner backing cavity (prevented by honeycomb cells), and that any perforations are closely spaced compared to a wavelength of sound. No end reflections are considered. That is, the soft duct is sufficiently long to render the reflections at the duct termination unimportant; or the mode is well enough cut on so that no end reflection will occur. A cut-on mode is defined here as a propagating mode; the frequency parameter (η) is sufficiently high so that axial propagation occurs. Only very near cut-off will this assumption (no end reflection) be a problem. Below cut-off the modes carry very little energy due to their out-of-phase pressure-velocity relationship and well above cut-off the end impedance (ref. 12) is such that very little reflection will occur. It is further assumed that the sound pressure level is sufficiently low so that the linearized acoustic wave equation is valid.

The acoustic wave equation is expressed as:

$$\nabla^2 p = \frac{1}{c^2}\frac{\partial^2 p}{\partial t^2} + \frac{2M}{c}\frac{\partial^2 p}{\partial x\,\partial t} + M^2\frac{\partial^2 p}{\partial x^2} \tag{1}$$

The geometric notation used is shown in figure 3. In the following paragraphs, the ∇^2 operator will be defined for Cartesian and cylindrical coordinate systems. If separation of variables solutions are sought in the form of

$$p = \sum_{j=1}^{\infty} p_j = \sum_{j=1}^{\infty} P_j e^{i\omega t-(\omega/c)(\sigma_j+i\tau_j)x} \tag{2}$$

where P_j is a function of the transverse dimensions (y, z or r, Φ) then, from the linearized momentum equations, the acoustic particle velocity can be expressed as:

$$v_j = \frac{i\nabla p_j}{\rho\omega Q_j} \tag{3}$$

where

$$Q_j = 1 + iM(\sigma_j + i\tau_j) \tag{4}$$

the j subscript is used to denote the infinite number of possible modal solutions.

Circular Duct

For a circular duct (cylindrical coordinates), the left side of equation (1) can be expressed as:

$$\nabla^2 p = \frac{1}{r}\frac{\partial}{\partial r}\left(r\frac{\partial p}{\partial r}\right) + \frac{1}{r^2}\frac{\partial^2 p}{\partial \Phi^2} + \frac{\partial^2 p}{\partial x^2} \tag{5}$$

The remaining term in equation (2) is then sought in the form

$$P_j(r, \Phi) = \mathscr{P}_j(r)e^{-im\Phi} \tag{6}$$

Thus, using equations (1), (2), (5), and (6) results in

$$r^2\frac{d^2\mathscr{P}_j}{dr^2} + r\frac{d\mathscr{P}_j}{dr} + \left[\left(\frac{\alpha_j r}{r_o}\right)^2 - m^2\right]\mathscr{P}_j = 0 \tag{7}$$

where

$$\left(\frac{\alpha_j}{r_o}\right)^2 = \frac{\omega^2}{c^2}\left[(1 - M^2)(\sigma_j + i\tau_j)^2 + i2M(\sigma_j + i\tau_j) + 1\right] \tag{8}$$

is the equation that links the eigenvalues (α_j) with the axial attenuation and propagation coefficients (σ, τ). Equation (7) is recognized as Bessel's differential equation with solution

$$\mathscr{P}_j(r) = J_m\left(\frac{\alpha_j r}{r_o}\right) + A_j Y_m\left(\frac{\alpha_j r}{r_o}\right) \tag{9}$$

where the α_j and A_j must be determined by radial boundary conditions. A second constant of integration which usually appears before J_m has been set equal to 1.

Equation (9) is valid for annular or open circular ducts. However, for added simplicity in this paper, the annular duct case (splitter rings) will be approximated by a rectangular duct development in the next section. Of immediate interest, however, is the case of an open circular duct. For this geometry, since $Y_m(\alpha_j r/r_o)$ becomes infinite as $r \to 0$, the condition must be imposed that

$$A_j = 0 \qquad \text{(all } j\text{)} \tag{10}$$

The remaining radial boundary condition involves the wall impedance at $r = r_o$. The acoustic impedance can be expressed as:

$$Z = \left.\frac{p}{v_{rw}}\right]_{r=r_o} \tag{11}$$

where v_{rw} is the radial velocity within the wall (axial velocity within the wall is assumed to be zero). Using continuity of radial particle displacement the radial particle velocity just outside the wall for the j^{th} radial mode is (ref. 14, p. 314, eq. (34)):

$$v_{rj} = Q_j v_{rwj} \tag{12}$$

Note that particle velocity continuity is not satisfied unless $Q_j = 1$ ($M = 0$). This is due to the artificial slip condition of the fluid at the wall. Using equations (2), (3), (6), (11), and (12) and defining a new normalized acoustic impedance there results

$$\zeta = \frac{Z}{\rho c} = \left[\frac{-i\pi\eta Q_j^2 \mathscr{P}_j}{r_o \dfrac{d\mathscr{P}_j}{dr}} \right]_{r=r_o} \tag{13}$$

where

$$\eta = \frac{fD}{c} \tag{14}$$

is the frequency parameter and D is the duct diameter. Using equations (9) and (10), equation (13) becomes:

$$\zeta = \frac{i\pi\eta Q_j^2 J_m(\alpha_j)}{\alpha_j J_{m+1}(\alpha_j) - m J_m(\alpha_j)} \tag{15}$$

from which the eigenvalues (α_j) can be determined for given wall impedance, lobe number (m), steady flow Mach number, duct size and frequency. If continuity of particle velocity had been used, Q_j would have appeared to the first power in equation (15).

The remaining necessary boundary conditions have been subtly satisfied due to the choice of solution forms in equations (2) and (6). Tangential continuity of pressure and velocity are satisfied if m is an integer in equation (6). Only positive x traveling waves are considered by the choice of the x function in equation (2); end reflections are neglected.

Rectangular Duct

Due to the relative simplicity of the sinusoidal functions compared to the Bessel functions, the annular duct (splitter ring case) will be approximated by a semi-infinite rectangular duct.

For a rectangular coordinate system the left side of equation (1) becomes:

$$\nabla^2 p = \frac{\partial^2 p}{\partial x^2} + \frac{\partial^2 p}{\partial y^2} + \frac{\partial^2 p}{\partial z^2} \tag{16}$$

The analogy to equation (6) is

$$p_j(y, z) = \mathscr{P}_j(y) e^{-imz/r_o} \tag{17}$$

where z/r_o has taken the place of Φ. The spinning wave pattern will repeat continuously over z distances equal to the outer circumference of the annulus.

As previously mentioned this rectangular duct solution should be a good approximation to the true annular solution if the radius of curvature is large and if the radius ratio is sufficiently close to 1. The conditions are usually satisfied at least for the outer passage of a splitter ring inlet which passage might be expected to carry most of the acoustic power.

Using equations (16), (17), and (2) in (1) results in:

$$\frac{d^2 \mathscr{P}_j}{dy^2} + \left(\frac{\alpha_j}{a}\right)^2 \mathscr{P}_j = 0 \tag{18}$$

where

$$\left(\frac{\alpha_j}{a}\right)^2 = \frac{\omega^2}{c^2}\left[(1 - M^2)(\sigma_j + i\tau_j)^2 + i2M(\sigma_j + i\tau_j) + 1 - \left(\frac{mc}{\omega r_o}\right)^2\right] \tag{19}$$

which links the eigenvalue (α_j) to the axial attenuation and propagation coefficients. Equation (18) has solutions

$$\mathscr{P}_j(y) = \cos\left(\frac{\alpha_j y}{a}\right) \quad \text{or} \quad \sin\left(\frac{\alpha_j y}{a}\right) \tag{20}$$

representing symmetric and asymmetric modes, respectively. Following a procedure analogous to equations (11) to (15) provides the wall impedance equations:

$$\zeta = \frac{i\pi\eta Q_j^2 \cos \alpha_j}{\alpha_j \sin \alpha_j} \tag{21}$$

for symmetric modes, and

$$\zeta = \frac{-i\pi\eta Q_j^2 \sin \alpha_j}{\alpha_j \cos \alpha_j} \tag{22}$$

for asymmetric modes where the impedance condition was applied at $y = \pm a$ and where now

$$\eta = \frac{\omega a}{\pi c} = \frac{fH}{c} \tag{23}$$

with H being the duct height between the two walls with acoustic treatment. Again equations (21) or (22) will provide the eigenvalues (α_j) when ζ, m, M, H, and f are provided.

Acoustic Power Attenuation

In the more general development where multimodal propagation is considered, the acoustic power attenuation is quite complicated (refs. 1 and 3). The complete pressure and the three velocity components must be constructed from the combination of all of the modes. The modal participation is determined by the input waveform from the noise source. The acoustic intensity is then determined and, since products of pressure and velocity are involved, modal cross coupling must be considered. The intensity must be integrated over the cross section at two axial stations, say $x = 0$ and L since the radial distribution of intensity may change with axial distance. Finally these integrated intensities which form the acoustic power can be used to determine an attenuation from:

$$\Delta \text{ dB} = 10 \log\left(\frac{E_{x=L}}{E_{x=0}}\right) \tag{24}$$

For the case of a single mode the situation is much simpler. Since a mode does not change relative shape as it travels down the duct, no integration is necessary. The procedure outlined above reduces to

$$\Delta \text{ dB} = 10 \log\left(e^{-2\omega\sigma_j L/c}\right) = -8.68 \frac{\omega\sigma_j L}{c} \tag{25}$$

or

$$\frac{\Delta \text{ dB}}{L/D} = -17.4\ \pi\eta\sigma_j \tag{26}$$

for circular ducts and

$$\frac{\Delta \text{ dB}}{L/H} = -17.4\ \pi\eta\sigma_j \tag{27}$$

for rectangular ducts. Although equations (26) and (27) look the same, the η terms are defined differently, and the σ_j will be different for rectangular and circular ducts.

The damping (σ_j) and propagation (τ_j) coefficients can be determined from equations (8) and (19) to be:

$$\sigma_j + i\tau_j \quad \frac{-iM + i\sqrt{1 - (1 - M^2)\left(\frac{\alpha_j}{\pi\eta}\right)^2}}{1 - M^2} \tag{28}$$

for circular ducts and

$$\sigma_j + i\tau_j = \frac{-iM + i\sqrt{1 - (1 - M^2)\left[\left(\frac{\alpha_j}{\pi\eta}\right)^2 + \frac{1}{M_t^2}\right]}}{1 - M^2} \tag{29}$$

for rectangular ducts. The last term under the radical in (29) was obtained from the expression

$$M_t = \frac{\omega r_o}{mc} = \frac{2\pi\eta}{m(1-\delta)} \tag{30}$$

which defines the tip Mach number of the spinning lobe pattern where δ is the equivalent annular duct radius ratio.

The calculation procedure and the results of the above theory for a single mode will now be presented followed by a return to the theory to obtain approximate solutions which will help explain the exact solutions.

CALCULATION PROCEDURE

The calculation procedure for cylindrical ducts will be outlined here. The rectangular duct procedure would follow a similar pattern except for the added simplification of having only sine and cosine functions. The method used to handle the Bessel functions with complex arguments will also be outlined.

Calculation of Maximum Attenuation and Optimum Impedance

The main complications center upon equation (15) which relates the infinite number of eigenvalues (α_j) to the normalized wall acoustic impedance (ζ). If a multimodal analysis were made (ref. 1) the impedance could be specified and the eigenvalues determined by iteration, series expansion, etc. For a single mode an inverse procedure greatly simplifies the problem. The eigenvalue is specified and the impedance can be immediately calculated. Since a major point of this paper was to determine the optimum impedance, this procedure was used. Considerable care was taken to insure that the selected eigenvalue belonged to the particular mode of interest.

For the actual calculations the starting point was one step removed from equation (15). Since contours of constant attenuation were desired and Δ dB is proportional to σ_j (eq. (26)), a value of σ_j was first assumed. A series of values of τ_j were then chosen which now defines the complex eigenvalue (α_j) through equation (8) or (28) which are versions of the same expression. The eigenvalue is then inserted into

equation (15) and the complex acoustic impedance is determined. The values of M, η, and m are held fixed for the calculation. These could later be varied to perform a complete parametric study.

A sample of the calculation results can be seen in figure 4 where lines of constant σ_j and τ_j are shown on the wall impedance plane. Note that both components of impedance have been divided by the frequency parameter η. This will make the plots similar for any η provided $M = 0$ or that the mode is well cut-on if $M \neq 0$. This last point will become more apparent in a later discussion. The initial calculation used a very small σ_j and a carefully selected τ_j to provide a large resistance and near-zero reactance (hard wall eigenvalues well known) to insure that the calculation was proceeding in the proper mode. The choice of τ_j will determine the mode for a fixed value of σ_j. The calculation then proceeds by increasing the value of σ_j until the teardrop-shaped constant damping curves degenerate to a point. This point then represents the optimum impedance for this mode and the value of σ_j determines the maximum possible sound power attenuation (from eq. (26)) for the given value of η. Actually only one value of η need be considered for the cases of most interest since the eigenvalue (α_j) at the optimum will not change with η. This fixed α_j can then be used to determine the maximum damping at any other η by using equations (28) and (26). The cases of most interest again are for $M = 0$ or that if $M \neq 0$ the mode is cut-on. This really means that Q_j in equation (15) and defined by equation (4) is not a function of η but can be approximated by:

$$Q_j \approx \frac{1}{1 + M} \tag{31}$$

for well cut-on modes or from equation (4) $Q_j = 1$ for $M = 0$ at any value of η. This will be derived in the discussion preceding equation (54).

If σ_j is pushed above the maximum defined above, one will find that the results generate a new set of contours collapsing to a point at some lower impedance, these contours representing the next higher radial mode.

The above procedure provides the maximum damping and optimum impedance for the least attenuated mode if the starting values of σ_j and τ_j are properly chosen.

Calculation of Complex Bessel Functions

The Bessel functions with complex argument could be calculated by the procedures given in reference 1. However, for the multitude of calculations required in the previous section it is most efficient to inspect one calculation before proceeding with the next. This requires the rapid communication which can conveniently be obtained from a desk calculator. The desk calculator often cannot handle the large subroutines required by the methods of reference 1. Thus the simplified procedures which follow were developed so that the Bessel functions themselves need not be calculated; only the ratio of two Bessel functions need be considered.

Equation (15) may be rewritten:

$$\zeta = \frac{i\pi\eta Q_j^2}{\alpha \dfrac{J_{m+1}(\alpha_j)}{J_m(\alpha_j)} - m} \tag{32}$$

The ratio J_{m+1}/J_m can be calculated as a single unit without ever considering each part. The Bessel function recursion relationship can be written (ref. 13):

$$J_{k-1}(\alpha_j) + J_{k+1}(\alpha_j) = \frac{2k}{\alpha_j} J_k(\alpha_j) \tag{33}$$

or

$$\frac{J_{k-1}(\alpha_j)}{J_k(\alpha_j)} = \frac{2k}{\alpha_j} - \frac{J_{k+1}(\alpha_j)}{J_k(\alpha_j)} \tag{34}$$

For any α_j, a sufficiently large value of k can be chosen so that the series representation of the Bessel function is rapidly convergent and the last ratio in (34) can be expressed as:

$$\frac{J_{k+1}(\alpha_j)}{J_k(\alpha_j)} \approx \frac{\alpha_j}{2(k+1)}\left[1 + \frac{\left(\frac{\alpha_j}{2}\right)^2}{(k+1)(k+2)} + \cdots\right] \tag{35}$$

If the first term of (35) is considered with large k it is seen to be approximately the inverse of and quite small compared to the first term of (34). In fact the second term of (34) could be neglected to start the recursion calculation although for this paper equation (35) was used. Equation (34) is repeatedly used with decreasing integers k until $k = m + 1$ and at each step the left hand side provides the inverse of the last term of (34) needed for the next step. Finally equation (34) provides the inverse of the Bessel function ratio needed in equation (32). This procedure provides excellent results with $k \approx 4|\alpha_j|$.

RESULTS OF SPINNING MODE PROPAGATION THEORY

The following sections present some results of the previously discussed sound propagation theory. The following discussion pertains to the least attenuated mode for a given spinning lobe number.

Circular Duct

In figure 5 the maximum possible attenuation for the least attenuated mode is shown as a function of the frequency parameter η. Several curves of constant lobe number (m = 0 to 50) are shown. Several loci of constant lobe pattern tip Mach numbers (M_t = 1 to 4) are also shown superimposed. This tip Mach number ($M_t = \pi\eta/m$) can be easily derived from lobe number, geometry, and frequency considerations.

The interesting point to note in figure 5 is that the maximum possible attenuation (peak attenuation for an optimized system) is a very strong function of the pattern lobe number (m), with larger values of m having larger values of attenuation. This may be the explanation for the apparently high experimental sound attenuations shown in figure 2 for circular ducts with wall treatment only. These data were high with respect to the axisymmetric theory (m = 0) but not necessarily high with respect to the spinning lobe theory.

It should be cautioned that a comparison of the data from figure 2 with the theory of figure 5 probably does not determine the spinning lobe number because the experimental suppressors were not necessarily optimized. Much higher experimental attenuations might have been attained with some other liner wall constructions.

The optimum wall impedance which goes along with the attenuations of figure 5 is given by:

$$\left.\begin{aligned} \theta &\approx \frac{B_\theta \eta}{(1 + M)^2} \qquad (36) \\ \chi &\approx \frac{B_\chi \eta}{(1 + M)^2} \qquad (37) \end{aligned}\right\} \quad \frac{R}{\pi\eta} < 1$$

with the coefficients B_θ and B_χ given in table I for various values of lobe number, and where R is obtained from $\alpha = Re^{i\varphi}$.

The corresponding eigenvalues at the optimum impedance are given in table II. Note that as the lobe number increases the optimum acoustic resistance (see B_θ) decreases and the optimum acoustic reactance (see B_χ) moves toward zero (the liner tuned frequency). This would imply that with spinning modes the peak attenuation would occur at a higher frequency (for a given liner construction) than would the axisymmetric mode. The approximations given in equations (36) and (37) are for well-cut-on modes with

$$\frac{R}{\pi\eta} < 1 \qquad (38)$$

where R is the magnitude of the eigenvalue for the mode. The locus of $R/\pi\eta = 1$ is shown in figure 5. The correction for steady flow Mach number will become apparent after a later discussion of approximate results.

It is apparent from the results shown in figure 5, by equations (36), (37), and table I that, for optimum design of circular duct acoustic suppression, much information must be known about the noise source. As a minimum at least the lobe number of the dominant mode must be known. Preferably the distribution of acoustic power within the radial modes should also be known, since radial modes other than the least attenuated mode would cause changes to be made in the numerical results of figure 5 and table I. The general conclusion that sound attenuation depends upon lobe number would not be changed for radial modes other than the least attenuated mode.

Rectangular Approximation to Annular Ducts

The results of the rectangular duct theory, intended to approximate the annular duct theory, are shown in figure 6. Again the maximum possible attenuation normalized by the duct L/H is shown as a function of frequency parameter $\eta = fH/c$. Several lobe tip Mach numbers and lobe numbers are shown. The lobe tip Mach number (M_t), frequency parameter (η), and lobe number (m) relationship shown on the figure comes from equation (30) with radius ratio $\delta = r_i/r_o = 0.8$.

In contrast to figure 5 for circular ducts, the rectangular duct theory shows that for moderately cut-on modes ($M_t \geq 1.4$) the spinning lobe theory collapses rapidly to the axisymmetric propagation theory ($m = 0$). Another way of viewing figure 6 is that for the usual range of interest for splitter ring suppressors ($1 \leq \eta \leq 2$), little difference in attenuation is observed between 20 lobes and zero lobes. Thus, the attenuation obtained from splitter ring suppressors is relatively insensitive to spinning lobe number if the modes are well cut-on.

The optimum wall acoustic impedance for the least attenuated spinning mode in a rectangular duct can be given by a single set of equations:

$$\left.\begin{aligned} \theta &\approx \frac{0.93\ \eta}{(1 + M)^2} \\ \chi &\approx \frac{-0.74\ \eta}{(1 + M)^2} \end{aligned}\right\} \frac{R}{\pi\eta} < 1 \tag{39, 40}$$

which are applicable for any lobe number (m). These equations again represent results for the least-attenuated mode. The optimum eigenvalue was given by $R \approx 2.364$ and $\varphi \approx 28$ degrees.

Thus, if a splitter ring inlet were being designed for the least-attenuated spinning mode and if this mode were well cut-on, the optimum liner design would be insensitive to the spinning lobe number as would be the attenuation. This interesting conclusion helps to explain the experimental results for splitter-ring inlets shown in figure 2. Although the noise may be distributed in spinning lobe patterns, the axisymmetric (m = 0) theoretical attenuation may be close to an upper limit for this type of suppressor.

The insensitivity of splitter-ring suppressor design and attenuation to spinning lobe number may also explain the quite good results obtained from previous suppressors in spite of the meager information available about the noise source.

Comments on Rectangular Approximation to Annular Duct

The use of the rectangular wave equation (eqs. (1) and (16)) to replace the more exact cylindrical coordinate system of the annular splitter ring passage should create no problem for the limited scope solutions of interest in this paper. For the high radius ratios of interest, curvature effects should be negligible. In reference 14 radius ratios from zero to about 0.8 were used in a cylindrical system with constant frequency parameter (η), and no change was found in the propagation or attenuation coefficients when $r_i/r_o > 0.4$. This implies that curvature effects were negligible above this radius ratio (0.4). In reference 14 only non spinning mode results were shown, and it is conceivable that

spinning modes with high spiral angles may be more sensitive to curvature. However, at least for well-cut-on spinning modes, there is very little spiral angle in a cylindrical duct which can be seen by looking at the axial phase velocity:

$$v_{px} \approx c(1 + M)\left[1 + \frac{(1 + M)}{2}\left(\frac{R}{\pi\eta}\right)^2 \cos 2\varphi\right] \tag{41}$$

or the axial group velocity:

$$v_{gx} \approx c(1 + M)\left[1 - \frac{(1 + M)}{2}\left(\frac{R}{\pi\eta}\right)^2 \cos 2\varphi\right] \tag{42}$$

which are respectively slightly greater and less than those of a plane wave (no spiral angle) in a hard duct which are both equal to $[c(1 + M)]$. This is true since $(R/\pi\eta)$ is small for a well cut-on mode.

Another problem does arise, however, with regard to what modal structure of sound is excited within the annular liner passages. The results of this paper are for the least attenuated mode in either the circular or annular duct. This represents the most conservative single mode result. The problem in the splitter ring passage can be illustrated in figure 7. The first radial mode (cylindrical coordinates) with small and large lobe numbers are sketched as input to the splitter ring passage. For small enough lobe number, the pressure is more uniform over the annulus and the least attenuated mode will dominate in the carrying of sound power. The results of this paper should be valid for this case. As lobe number is increased, more higher radial mode content will be excited in the annulus, and the least attenuated mode approximation will underestimate the true attenuation because these higher radial modes have higher damping coefficients.

If the lobe number is increased even further (dashed line, fig. 7), the pressure amplitude at the splitter ring will approach zero, and the ring will be completely ignored in the sound propagation. For this case the open circular duct (no splitter rings) solution will become valid. This can be further emphasized by repeating equation (9)

$$\mathscr{P}_j(r) = J_m\left(\frac{\alpha_j r}{r_o}\right) + A_j Y_m\left(\frac{\alpha_j r}{r_o}\right) \tag{9}$$

which represents an annular duct solution, and observing the value of A_1 (first radial mode) in figure 8. Figure 8 results are from reference 15 for hard wall annular ducts. For a given radius ratio (δ), as the lobe number (m) is increased, A_1 rapidly drops toward zero. Of course as $A_1 \to 0$, the open circular duct solution is approached, that is:

$$\mathscr{P}_j(r) \to J_m\left(\frac{\alpha_j r}{r_o}\right) \tag{43}$$

and the presence of the splitter ring becomes irrelevant to the solution. The same phenomenon occurs for higher radial modes but at higher lobe numbers. This type of modal pressure distribution may account for the noise suppressor data at low frequencies shown in figure 1. Recall that for frequencies of about 1000 hertz and lower, the splitter rings produced very little added attenuation.

INTERPRETATION OF THEORETICAL RESULTS USING APPROXIMATE EXPRESSIONS

It is useful to derive approximate expressions from the preceding theoretical analysis to clarify the basic difference between noise suppressors with splitter rings and with wall treatment alone. Approximations stated earlier without proof will be derived here. The approximations are mainly for well cut-on modes, which are of the most interest, since they carry the bulk of the acoustic power.

Well Cut-on Modes

Some preliminary approximations are required; the first being applied to equation (29) for the damping and propagation coefficients

for rectangular ducts. The subscripts will be dropped and it will be understood that the least attenuated mode will be considered.

$$\sigma + i\tau = \frac{-iM + i\sqrt{1 - (1 - M^2)\left[\left(\frac{\alpha}{\pi\eta}\right)^2 + \frac{1}{M_t^2}\right]}}{(1 - M^2)} \tag{29}$$

For a well cut-on mode:

$$(1 - M^2)\left[\left(\frac{\alpha}{\pi\eta}\right)^2 + \frac{1}{M_t^2}\right] << 1 \tag{44}$$

which allows the approximate expression

$$\sqrt{1 - x} \approx 1 - \frac{x}{2} \qquad (x << 1) \tag{45}$$

to be used. Also use:

$$\alpha^2 = R^2 e^{i2\varphi} = R^2(\cos 2\varphi + i \sin 2\varphi) \tag{46}$$

Therefore (29) can be written:

$$\sigma + i\tau \approx \frac{1}{2}\left(\frac{R}{\pi\eta}\right)^2 \sin 2\varphi + i\left\{\frac{1}{1 + M} - \frac{1}{2}\left[\left(\frac{R}{\pi\eta}\right)^2 \cos 2\varphi + \frac{1}{M_t^2}\right]\right\} \tag{47}$$

The damping coefficient is thus:

$$\sigma \approx \frac{1}{2}\left(\frac{R}{\pi\eta}\right)^2 \sin 2\varphi \tag{48}$$

and the propagation coefficient is:

$$\tau \approx \frac{1}{1+M} - \frac{1}{2}\left[\left(\frac{R}{\pi\eta}\right)^2 \cos 2\varphi + \frac{1}{M_t^2}\right] \tag{49}$$

For circular ducts equation (28) can be seen to be the same as equation (29) except that the M_t term is missing, and the lobe pattern tip Mach number information is in the $(\alpha/\pi\eta)^2$ term. For circular ducts the equations can be immediately determined from (48) and (49) by neglecting the M_t term.

$$\sigma \approx \frac{1}{2}\left(\frac{R}{\pi\eta}\right)^2 \sin 2\varphi \tag{50}$$

$$\tau \approx \frac{1}{1+M} - \frac{1}{2}\left(\frac{R}{\pi\eta}\right)^2 \cos 2\varphi \tag{51}$$

Note that the Mach number (M) has cancelled out of the damping equations (48) and (50). It will be shown shortly that the eigenvalue ($\alpha = Re^{i\varphi}$) is constant at the optimum point (limiting contour in fig. 4) even with a steady-flow Mach number. Thus, the maximum possible attenuation is not a function of Mach number but depends only upon the frequency parameter η.

Another approximation required is for the Q_j term in the wall impedance equations. This was given in equation (4) as: (again dropping subscripts)

$$Q = 1 + iM(\sigma + i\tau) \tag{52}$$

Note that in equation (47) the eigenvalue had to be carried to second power to get the damping coefficient σ. However, for well cut-on modes equation (47) is dominated by:

$$\sigma + i\tau \approx \frac{i}{1+M} \tag{53}$$

thus equation (52) can be estimated by

$$Q \approx \frac{1}{1 + M} \qquad \left(\frac{R}{\pi \eta} < 1\right) \tag{54}$$

Equation (54) can now be used in the wall impedance equations (21) and (15) to provide

$$\frac{\zeta(1 + M)^2}{\eta} \approx \frac{i\pi \cos \alpha}{\alpha \sin \alpha} \tag{55}$$

for rectangular ducts and

$$\frac{\zeta(1 + M)^2}{\eta} \approx \frac{i\pi J_m(\alpha)}{\alpha J_{m+1}(\alpha) - m J_m(\alpha)} \tag{56}$$

for circular ducts.

Rectangular approximation to annular ducts. - Some interesting conclusions can be drawn from equation (55) for rectangular ducts. Consider the left side as an effective impedance and note that the right side is a function only of the eigenvalue. Thus, an optimization procedure as explained in the CALCULATION PROCEDURE section and as shown in figure 4 need be done only once if the coordinates in figure 4 are considered as effective impedance instead of as impedance only. The eigenvalue (α) at which the constant σ contours collapse to a point (optimum effective impedance) will always be the same. Since $\alpha = Re^{i\varphi}$ is always constant at the optimum effective impedance, the conclusion stated after equation (51) is now justified. Since the damping coefficient (σ in eq. (48)) is not a function of Mach number (M) and α is constant, the optimum damping is a function only of the frequency parameter η. To carry this conclusion one step further, from equation (27) the normalized maximum possible attenuation (Δ dB/L/H) is a function only of the frequency parameter η for well cut-on modes and is given by

$$\frac{\Delta \text{ dB}}{L/H} \approx \frac{12.8}{\eta} \tag{57}$$

where the optimum rectangular eigenvalue ($R = 2.364$, $\varphi = 28^\circ$) was used.

Going back to equation (55) if the optimization procedure is performed at $M = 0$ and $\eta = 1$ it is found that

$$\zeta = 0.93 - i\,0.74 \tag{58}$$

thus in general

$$\zeta \approx \frac{(0.93 - i\,0.74)\eta}{(1 + M)^2} \tag{59}$$

which justifies equations (39) and (40).

Recall that the lobe number (m) did not occur either in the damping coefficient (eq. (48)) or in the wall impedance (eq. (55)). Thus for well cut-on modes the maximum possible attenuation and the optimum wall impedance are not functions of the spinning lobe number, a result which was also shown by the more exact theoretical results.

Circular ducts. - Some important differences between circular and rectangular ducts can be deduced from the approximate equations. For circular ducts the right hand side of the effective impedance Eq. (56) is seen to be a function of the lobe number (m). Thus although the optimization procedure of Fig. 4 can be performed for $M = 0$ and $\eta = 1$ and then applied to all M and η, the procedure must be repeated for each value of lobe number (m) of interest. This results in the optimum impedance coefficients of table I and the optimum eigenvalues of table II being functions of lobe number. This also implies through equations (50) and (26) that the normalized maximum possible attenuation (Δ dB/L/D) is a function of lobe number. It is still not a function of steady flow Mach number for $R/\pi\eta < 1$ in figure 5. Equations (27) and (50) can be combined to yield

$$\frac{\Delta\ \mathrm{dB}}{L/D} \approx \frac{D_m}{\eta} \tag{60}$$

where D_m is an attenuation coefficient dependent upon lobe number (m) and is given in table III.

Note that equation (60) used in conjunction with table III yields an approximation for large values of the frequency parameter (η). This inverse function is valid for the portions of the curves in figure 5 which are straight lines.

Cut-off Modes

When a mode is cut-off it is of less interest since it carries no power and is attenuated in even a hard walled duct. For completeness of the approximate equations, the attenuation of the cut-off modes will be developed. The $(\alpha_j/\pi\eta)^2$ term in equation (28) or (29) will dominate the radical and with $M = 0$ the result will be:

$$\sigma \approx \frac{R \cos \alpha}{\pi \eta} \tag{61}$$

for either rectangular or circular ducts.

Using equations (26) or (27) yields

$$\frac{\Delta \text{ dB}}{L/\beta} \approx -17.4 \, R \cos \alpha \tag{62}$$

where $\beta = D$ for circular ducts and $\beta = H$ for rectangular or annular ducts. Note that this expression does not contain the frequency parameter η and represents the horizontal portions of the curves in figures 5 and 6. This behavior has been observed before in references 16, 1, and 2. For $M = 0$ the same eigenvalues given following equation (40) for rectangular ducts and in table II for circular ducts can be used. However for $M \neq 0$, the situation is much more complicated. The simple expression (eq. (54)) for Q in the wall impedance equation is no longer valid. Q will be a function of η, and instead of just a simple stretching or compression of the equal damping curves in the impedance plane (see fig. 4) a rotation will also occur. The eigenvalues will thus be changed from those of a well cut-on mode.

An example of the effect of Mach number on the maximum possible attenuation for the least attenuated mode in rectangular ducts can be

found in figure III-13 (p. 87) of reference 4. It should be noted that only at low values of frequency parameter is this maximum attenuation a function of Mach number where attenuation increases for inlets and decreases for exhaust ducts. For $\eta > R/\pi$ this Mach number dependence vanishes as previously discussed.

CONCLUDING REMARKS

This paper could be briefly summarized as follows. Suppressors with outer wall treatment alone have been observed to provide much more attenuation than previously expected. Such expectations were based upon the extrapolation from splitter ring suppressor measurements or least attenuated axisymmetric, circular duct theory. The theoretical analysis of the least attenuated spinning mode with sound absorbing walls has revealed that the experimental results could have been anticipated qualitatively. Approximate expressions for the attenuation of well cut-on modes were presented to illustrate the theoretical results. To further pursue this approach more information is required about the spinning modal structure of the sound emanating from the source.

It was consistent with the spirit of this paper, then, to make all necessary assumptions required to point out as simply as possible the gross behavior of both splitter ring and wall only suppressors. Many of the conclusions made here could possibly be challenged by postulating modes near cut-off or more complex radial mode structures. However, the experimental data do provide credibility, if not precision, to the assumptions made here.

CONCLUSIONS

Within the restrictions of the assumptions made within this paper the following conclusions were made:

1. Noise suppressors with splitter rings are relatively insensitive to the spinning mode lobe number. This explains why quite simple non-spinning mode theory and rectangular flow duct tests have provided quite

predictable splitter ring designs in the past even where spinning modes were possible.

2. Circular noise suppressors with wall treatment only are very sensitive to spinning mode lobe number. This explains why axisymmetric cylindrical duct theory does not agree well with experimental data taken with fan noise sources.

3. Due to conclusion 2 above, much more detailed information about the fan noise source will be required to best take advantage of the great potential of wall-treatment-only suppressors.

4. Approximate expressions for sound attenuation for well cut-on modes have been presented which provide insight into the difference between the two types of suppressors.

5. In a splitter ring suppressor (or an annular exhaust duct), the presence of the inner wall can under some circumstances be completely ignored by the propagating spinning mode. This will occur when the radial pressure distribution is skewed toward the outer wall and very little pressure oscillation occurs on the inner wall. A high spinning lobe number and low radial mode will cause this to occur.

REFERENCES

1. E. J. Rice: Attenuation of Sound in Soft-Walled Circular Ducts. H. S. Ribner, ed., Aerodynamic Noise (Univ. of Toronto Press, 1969), pp. 229-249.

2. C. E. Feiler, E. J. Rice, and L. J. Smith, "Performance of Inlet Sound Suppressors," in Progress of NASA Research Relating to Noise Alleviation of Large Subsonic Jet Aircraft, NASA SP-189, 53-62 (1968).

3. E. J. Rice, "Propagation of Waves in an Acoustically Lined Duct with a Mean Flow," in Basic Aerodynamic Noise Research, NASA SP-207, 345-355 (1969).

4. C. E. Feiler, J. F. Groeneweg, E. J. Rice, E. B. Smith, and R. H. Tucker, "Fan Noise Suppression," in Aircraft Engine Noise Reduction, NASA SP-311, 63-102 (1972).

5. J. M. Tyler and T. G. Sofrin, "Axial Flow Compressor Noise Studies," SAE Trans., 70, 309 (1962).

6. P. M. Morse and K. U. Ingard, Theoretical Acoustics (McGraw-Hill Book Co., 1968).

7. M. E. Goldstein, J. H. Dittmar, and T. F. Gelder, "Combined Quadrupole-Dipole Model for Inlet Flow Distortion Noise from a Subsonic Fan," NASA TN D-7676 (1974).

8. M. J. Benzakein, R. E. Kraft, and E. B. Smith, "Sound Attenuation in Acoustically Treated Turbomachinery Ducts," ASME Paper 69-WA/GT-11 (Nov. 1969).

9. M. J. Benzakein and J. W. Zwick, "Sound Transmission and Suppression in Turbomachinery Ducts," ASME Paper 70-GT-58 (May 1970).

10. H. E. Plumblee, P. D. Dean, G. A. Wynne, and R. H. Burrin, "Sound Propagation in and Radiation from Acoustically Lined Flow Ducts: A Comparison of Experiment and Theory," NASA CR-2306 (1973).

11. S. B. Kazin and J. E. Pass, NASA/GE Quiet Engine C Acoustic Test Results. General Electric Co. Rept. R73AEG364 (Apr. 1974) also NASA CR 121176.

12. C. L. Morfey, "A Note on the Radiation Efficiency of Acoustic Duct Modes," J. Sound Vib., 9, 367 (1969).

13. F. B. Hildebrand, Advanced Calculus for Engineers (Prentice-Hall, Inc., 1949).

14. P. Mungur and H. E. Plumblee, 'Propagation and Attenuation of Sound in a Soft-Walled Annular Duct Containing a Sheared Flow," in Basic Aerodynamic Noise Research, NASA SP-207, 305-327 (1969).

15. John W. Converse and Joe D. Hoffman, Acoustic Standing Waves in a Rocket Combustion Chamber with Ring and Spoke Baffles. Jet Propulsion Center Rept. JPC-436 (Aug. 1967).

16. V. L. Cremer, "Theory of Sound Attenuation in a Rectangular Duct with an Absorbing Wall and the Resultant Maximum Coefficient," Acustica, 3, 249 (1953).

TABLE I. - OPTIMUM RESISTANCE AND REACTANCE COEFFICIENTS FOR SPINNING MODES IN CIRCULAR DUCTS

m	0	1	3	5	7	10	20	50
B_θ	0.890	0.644	0.448	0.357	0.303	0.251	0.170	0.097
B_χ	0.38	0.221	0.121	0.095	0.076	0.060	0.038	0.020

TABLE II. - EIGENVALUES AT OPTIMUM IMPEDANCE FOR SPINNING MODES IN CIRCULAR DUCTS

m	0	1	3	5	7	10	20	50
R	3.278	4.691	7.299	9.759	12.088	15.547	26.662	58.620
φ, deg	23.19	18.07	13.49	10.91	9.75	8.03	5.46	3.32

TABLE III. - COEFFICIENT FOR MAXIMUM POSSIBLE ATTENUATION, SPINNING MODES, CIRCULAR DUCT

m	0	1	3	5	7	10	20	50
D_m	21.51	35.88	66.83	97.87	134.9	184.9	372.3	1099

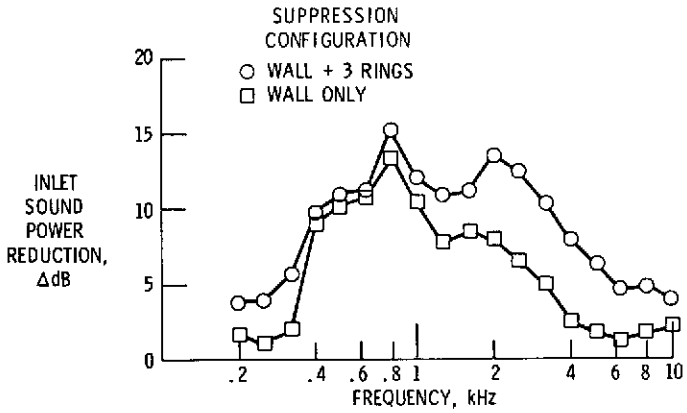

Figure 1. - Effect of inlet suppressor configuration on sound power attenuation. (Fan C, 90% speed.)

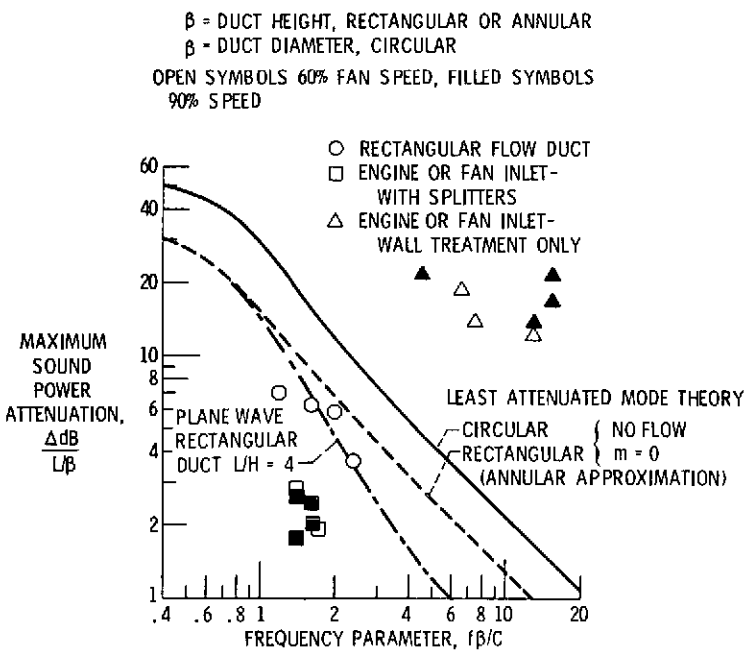

Figure 2. - Comparison of suppressor theory and data.

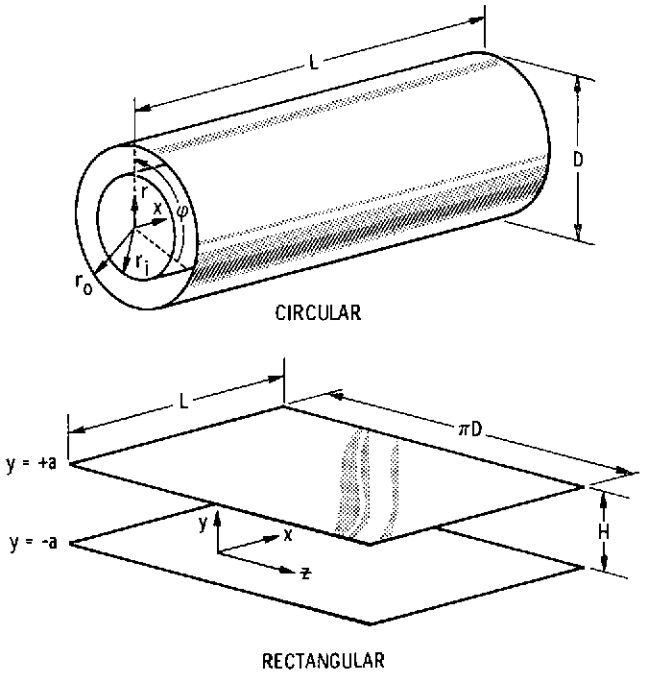

Figure 3. - Geometry for analytical models.

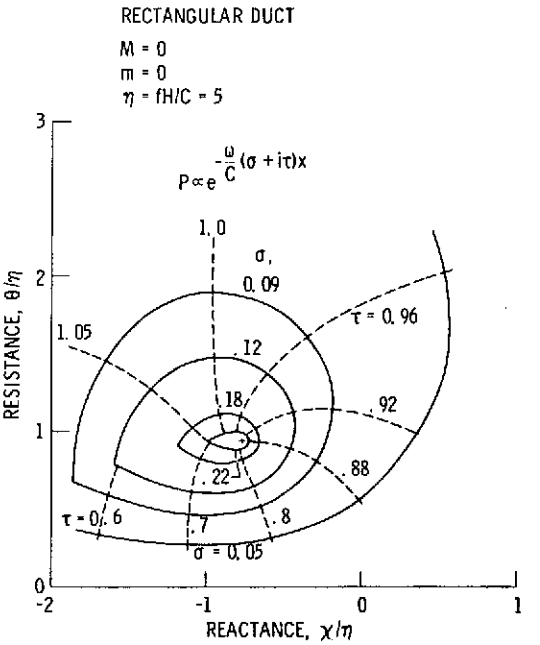

Figure 4. - Sample results showing optimum impedance definition.

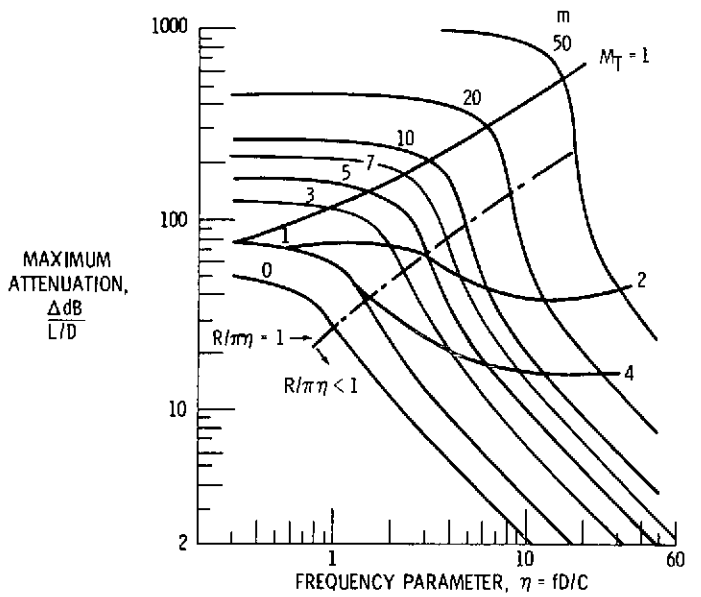

Figure 5. - Maximum attenuation for least attenuated spinning modes in circular duct. M = 0.

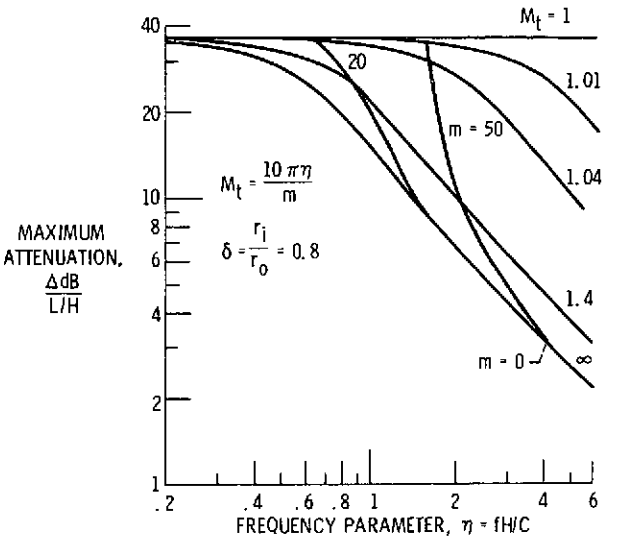

Figure 6. - Maximum attenuation for least attenuated spinning modes for rectangular approximation to annular duct.

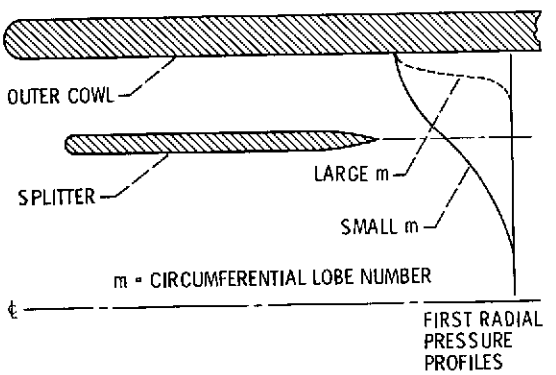

Figure 7. - Pressure profiles as a function of lobe number.

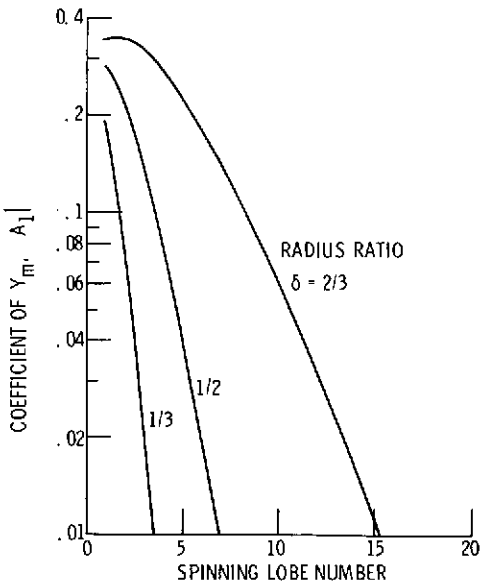

Figure 8. - Coefficient of Bessel function (Y_m) related to lobe number and radius ratio for annular ducts with hard walls.